Volume 1 | Number 1 | Jan 2013 | Pages 1–100

Journal of
Materials Chemistry A

Materials for energy and sustainability
www.rsc.org/materialsA

Li⁺

ROYAL SOCIETY OF CHEMISTRY

ROYAL SOCIETY OF CHEMISTRY

www.rsc.org/materialsA

Journal Name

ARTICLE

Surface etching of HKUST-1 promoted via supramolecular interactions for chromatography

Samir El-Hankari[a], Jia Huo[a], Adham Ahmed[b], Haifei Zhang[b] and Darren Bradshaw*[a]

The addition of guanidinium-based surfactants to the synthesis of HKUST-1 reveals a novel surface patterning effect where meso- and macroscopic features appear on the MOF crystals. The size of the features increases with increasing alkyl chain length of the guanidinium amphiphiles, and their formation is strongly dependent on the presence of water which appears to more favourably etch the crystal surfaces when the surfactants are employed. The patterned crystals display intermediate type I/IV isotherms and the presence of the surface features have been evaluated for the chromatographic separation of styrene and ethylbenzene. Some degree of control over the interactions between the framework building blocks and the amphiphiles is afforded, and by simply changing the order of addition of the reactants the guanidinium surfactants promote the formation of HKUST-1 nanoparticles.

Introduction

Metal-organic frameworks (MOFs) are functional crystalline highly porous network structures prepared by the assembly of metal ions with suitable multitopic organic linking groups.[1] They are characterised by high internal surface areas, and the relative ease by which their pore metrics and other physical properties can be modulated for applications such as gas storage[2], catalysis[3], drug delivery[4], sensing[5] and separation[6] ensure these materials are highly technologically relevant. Their properties are often further enhanced through processing of MOFs and MOF-based composites into application-specific configurations.[7]

At present the vast majority of MOFs are classed as microporous with pore dimensions typically < 2 nm in diameter. While this relatively small pore size is ideal for the separation and catalysis of small molecules with high selectivity, this necessarily places some restrictions on their practical use. For example, the micropores present a high diffusion barrier to species entering or leaving the frameworks and will ultimately limit the use of MOFs to the separation and catalysis of small molecules. To enhance their utility in these and other applications there is thus a great need to increase the pore size of MOFs. As alternatives to increasing the micropore size of the framework through expanded building blocks[8], which tend to lead to interpenetrated frameworks of reduced porosity or materials which are less stable to activation, soft templating using supramolecular assemblies[9], gelation to form MOF aerogels[10], crystal etching[11] and transformation of mesoscopic oxides[12] are all emerging as very promising strategies.

Amphiphilic surfactant species have proven versatile to drive MOF pore sizes into the mesoporous regime, where they play a structure-directing[13] or space-filling[14] role. The microporous frameworks either assemble around large supramolecular aggregates of surfactants or crystal-growth is

precluded in certain regions by the long-alkyl chains, which both result in the formation of large pores within the MOF particles. In each case a strong interaction between the (polar) amphiphile headgroup and the metal ions and/or ligands required for MOF formation is essential.
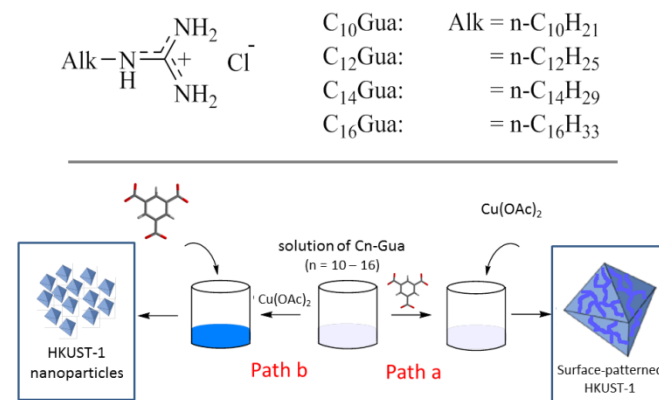
Scheme 1. (Top) Structure of the guanidinium surfactants (CnGua) used in this work. (Bottom) Representation of the synthesis of HKUST-1 in the presence of CnGua. Path a initially adds the BTC linker to the surfactant solution prior to solvothermal reaction, which results in meso-/macroscale patterning of the surface of HKUST-1 microcrystals. Reversing the order of addition however leads to MOF nanocrystals (path b).

In this work we have investigated the effect of long chain guanidinium species (scheme 1, top) on the pore and crystal size of the prototypical HKUST-1 framework[15], a stable carboxylate-based MOF of formula $Cu_3(BTC)_2(H_2O)_2$ (BTC = 1,3,5-benzenetricarboxylate) that has found widespread application in catalysis and separation.[11a, 16] The guanidinium group was specifically selected due to its rich supramolecular chemistry with sulphonate and carboxylate functionalities, which has led to the formation of diverse hydrogen-bonded

structures including cages[17], clathrates[18], rosette-type networks[19] and porous organic solids containing well-defined water channels.[20] Long chain guanidinium amphiphiles have also been employed for the preparation of nanostructured mesoporous silica[21], and their potential to endow HKUST-1 with larger pores via a templating or space-filling effect has thus been evaluated.

During the course of this work we have discovered a novel patterning effect for HKUST-1 crystals formed only in the presence of guanidinium surfactants (scheme 1, path a), where large meso- and macroscale features are clearly identifiable on the crystal faces. These surface features arise from increased etching by atmospheric moisture promoted by an increase in (surface) defects arising directly from supramolecular interactions with the guanidinium species during framework formation. The surface features affect the adsorption properties of the materials, which have been further investigated for their potential as stationary phases in high performance liquid chromatography (HPLC). The order of addition of the framework-forming components is also found to be important, and in addition to the formation of crystals with well-defined surface features, HKUST-1 nanoparticles are also accessible from this reaction system (scheme 1, path b).

Experimental

Materials synthesis

1H-Pyrazole-1-carboxamidine hydrochloride, the primary alkyl amines, 1,3,5-benzenetricarboxylic acid (BTC), Copper(II) acetate monohydrate ($Cu(OAc)_2 \cdot H_2O$) and absolute ethanol were purchased from Sigma-Aldrich and used without further purification. Ultrapure Milli-Q water (Milli-Q System, Millipore, Billerica, MA) was used in all experiments. The alkyl guanidinium chlorides were synthesised from the corresponding primary alkylamines according to a recently reported procedure.[21]

Preparation of C_nGua-HKUST-1. The guanidinium surfactant (C_nGua) 0.3 mmol was dissolved in 6.66 g of water and stirred at 50 °C for 1 h. 0.25 g (1.2 mmol) of BTC dissolved in 3 g of absolute ethanol was then added to the aqueous C_nGua solution, and stirred at 50 °C for a further 20 min after which time 0.4 g (2 mmol) of $Cu(OAc)_2 \cdot H_2O$ was added. A blue precipitate formed immediately. The heterogeneous mixture was vigorously stirred for an extra 5 min and then heated in a sealed autoclave at 120 °C for 22 hours. After this time, the mixture was cooled to room temperature, and the formed solid was isolated by filtration and dried in air. Finally, the surfactant was eliminated by washing 0.3 g of the MOF-C_nGua composite in 60 ml of EtOH at 60 °C.

Synthesis of nanoHKUST-1 in the presence of $C_{12}Gua$. The same molar quantities of $C_{12}Gua$, BTC and Cu(OAc) were employed for the synthesis of $C_{12}Gua$-HKUST-1 were used, except the order of addition between the metal salt and ligand was reversed. In a glass bottle of 50 ml, $C_{12}Gua$ was dissolved and stirred in water at AT for 10 min, then Cu(OAc)$_2$ is added to the solution of surfactant and stirred for another 1h, during which time a precipitate is formed. BTC (0.25 g, 2 mmol) is added and the heterogeneous mixture vigorously stirred for 5 min. The above suspension was poured into a Teflon-lined stainless steel autoclave of 20 mL capacity, sealed and heated to 120 °C for 22h. After cooling to ambient the blue precipitate was collected, washed with ethanol several times to remove any unreacted species and dried in air before washing as described above.

Materials characterisation

All samples were examined by powder X-ray diffraction (PXRD) in the angular range $2\theta = 5 - 40^o$ using a Bruker D2 phaser employing a Ni Kβ filter (detector side) producing Cu (Kα1/Kα2) radiation. The morphologies and structures were visualised with scanning electron microscopy (SEM) measurements on a JEOL JSM 6500F field-emission SEM at an accelerating voltage of 15 kV. N_2 adsorption–desorption isotherms were collected using a Micromeritics 3-Flex at 77 K. The samples were first degassed at 110 °C overnight. Surface areas were determined by the BET method in an appropriate pressure range. The meso- or macropore size distribution was calculated using the Barrett-Joyner-Halenda (BJH) method. Thermogravimetric analysis (TGA) was performed using a Perkin Elmer STA6000 Simultaneous Thermal Analyzer and the sample was heated from room temperature to 800 °C at a rate of 10 °C min^{-1} under an O_2 atmosphere.

Results and discussion

HKUST-1 was prepared in the presence of amphiphilic guanidinium chloride salts with alkyl chain lengths from $C_{10} - C_{16}$ ($C_{10}Gua - C_{16}Gua$) as shown in scheme 1. Two methods were employed by varying the order of addition of the framework-forming components resulting in surface-patterned crystals or nanoparticles, by adding first the ligand or metal salt respectively, to the surfactant solution.

Surface patterning of HKUST-1 by C_nGua

Given the strong directional electrostatic interactions between guanidinium and deprotonated carboxylic acids[19] the surfactants were first stirred only in the presence of the BTC linker to promote their supramolecular organisation prior to addition of the metal salt. (Scheme 1a) The typical molar ratio of C_nGua:BTC was 1:4 and these were stirred in a water/EtOH solvent mixture at 50°C for 20 mins, after which time 1.6 equivalents (wrt BTC) of hydrated $Cu(OAc)_2$ was added. Following solvothermal treatment at 120 °C, the resulting blue powders were isolated by filtration and washed to remove any surfactant species bound to the surface of the crystals. The obtained materials are labelled as C_nGua-HKUST-1 (where n= 10, 12, 14 and 16; the carbon chain length of the surfactant).

Powder X-ray diffraction (PXRD) patterns of C_nGua-HKUST-1 phases (Fig. S1) are in excellent agreement with that of pure HKUST-1; hence the presence of the C_nGua surfactants in the synthesis mixture does not adversely affect MOF assembly. The morphologies of C_nGua-HKUST-1 crystals were visualized by scanning electron microscopy (SEM) as shown in figure 1. While the C_nGua-HKUST-1 crystals maintain the expected octahedral block morphology observed for bulk HKUST-1, the SEM images clearly reveal the presence of meso- and macroscale patterns on the surface of the 0.2 – 0.4 µm-sized crystals in all of the products prepared with C_nGua.

The size of the surface features appear to increase as the chain length of C_nGua increases: only small barely identifiable features are observed on the surface of $C_{10}Gua$-HKUST-1 (fig. 1c,d), whereas deeper macroscopic trenches are present on crystals of $C_{16}Gua$-HKUST-1 (fig. 1i,j). This is in contrast to the smooth surfaces observed for HKUST-1 formed under the same conditions in the absence of the C_nGua surfactants (fig. 1a,b), strongly suggesting that interactions between the cationic Gua headgroup and the BTC framework-forming linker play a clear role in the patterning process where alkyl chain length appears to further affect feature size.
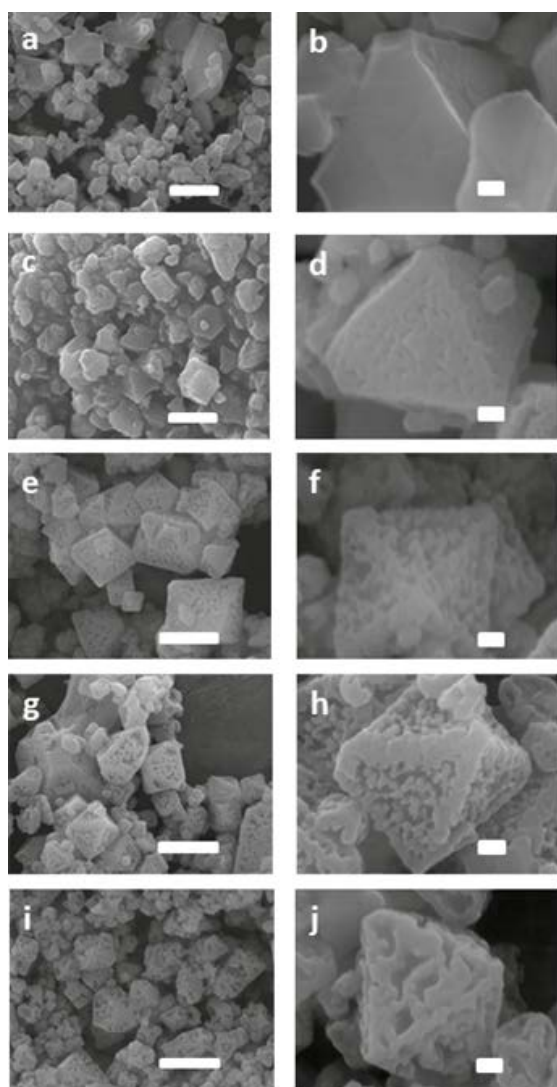
Figure 1. SEM images of HKUST-1 prepared in the absence of (a, b) and presence of C_nGua surfactants: n = 10 (c, d); n = 12 (e, f); n = 14 (g, h) and n = 16 (i, j). Scale bars are 1 μm (a, c, e, g, i) and 100 nm (b, d, f, h, j).

The C_nGua-HKUST-1 materials were further characterized by N_2 adsorption-desorption isotherms to determine additional information regarding their surface textures. (Figure 2) In contrast to the type I isotherm characteristic for microporous HKUST-1, all C_nGua-HKUST-1 phases displayed intermediate type I/IV isotherms with pronounced N_2 uptake at relative pressures ≥ 0.90 consistent with the presence of the meso- and macroscale features on the MOF crystal surfaces identified by SEM. As summarized in table S1, the pore sizes extend into the macroporous regime with pore diameters in the range 53–73 nm in addition to the HKUST-1 micropores. The apparent BET surface areas (table S1) and micropore uptakes (at $p/p^0 = 0.3$) of C_nGua-HKUST-1 both decrease as alkyl chain length of C_nGua increases, and in all cases are lower than observed for bulk HKUST-1.

The reduced (micro)porosity implies the presence of residual C_nGua surfactants in the pores of the framework or adsorbed to the crystal surface, blocking access to the micropores of the framework. The presence of C_nGua has been identified by ES-MS (fig S2) following acid digestion of

C_nGua-HKUST-1 after washing in EtOH at 60 °C, confirming the strong nature of the interactions between the surfactant and the carboxylate groups of the BTC linker. The amount of remaining C_nGua was quantified by thermogravimetric analysis (TGA) (fig. S3 – S6) which reveals this is typically ≤ 1.5 wt % after washing, where the total mass losses observed for C_nGua-HKUST-1 are almost identical to HKUST-1 itself. The very low residual amount of C_nGua was further confirmed by FTIR, since this was only observable in a control sample of HKUST-1 deliberately containing 20 wt% of the surfactant. (Fig. S7) Although partial pore blockage by C_nGua species cannot be totally ruled out, it is unlikely that such a small residual quantity of surfactant is wholly responsible for the observed significant reduction of porosity, and it is noted that a similar effect is found for HKUST-1 phases exposed to humid atmospheres arising from partial degradation of the structure via surface reconstruction.[22a] This suggests that the surfaces of the C_nGua-HKUST-1 phases could be more susceptible than bulk HKUST-1 to attack by adventitious water upon standing.
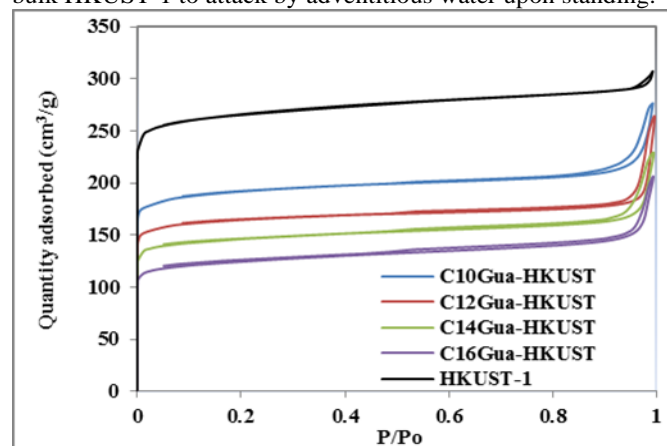

Figure 2. N_2 adsorption-desorption isotherms at 77K for C_nGua-HKUST-1 phases prepared in the presence of Gua surfactants compared to bulk HKUST-1.

Interestingly, the surface features highlighted in fig. 1c-j are not present on the C_nGua-HKUST-1 crystals immediately following synthesis (figure S8), where smooth facets reminiscent of the HKUST-1 crystals shown in fig 1a, b are observed. Indeed the C_nGua-HKUST-1 crystals shown in fig 1c-j were imaged after 30 days exposure to the laboratory atmosphere, indicating that the patterning does not result only from a simple templating or space-filling effect by the C_nGua surfactants during synthesis and that another step is clearly involved. The moisture sensitivity of HKUST-1 is extremely well documented[22,23] and given the reduced porosity and almost total absence of residual C_nGua determined by N_2 adsorption (fig 1, table S1) and TGA (fig S3 – S6) respectively, we investigated the specific role played by water in the surface patterning of C_nGua-HKUST-1. It is further noted that similar meso- and macroscopic features have been observed following post-synthetic etching of IRMOF-3 in basic solutions of cyanuric chloride.[24]

Role of moisture in surface patterning of C_nGua-HKUST-1

To determine the role of atmospheric moisture in forming the surface patterns on C_nGua-HKUST-1, the crystals were stored in a laboratory desiccator under atmospheres of both high and low moisture contents relative to our laboratory atmosphere *i.e.* with and without water present in the desiccator, respectively (fig S9). After storing $C_{12}Gua$-HKUST-

1 and C$_{14}$Gua-HKUST-1 in a higher humidity atmosphere for 60 days, these materials undergo structural changes as evidenced by PXRD and SEM (fig S10, S11) and as previously observed for HKUST-1.[22, 23] Indeed the appearance of a second phase and almost total absence of surface features indicate that framework degradation under high moisture conditions is dominant and hence the role played by water in (surface) patterning cannot be unambiguously evaluated in saturated atmospheres.

To reduce atmospheric moisture and monitor the evolution of the surface features, washed as-made crystals of C$_{12}$Gua-HKUST-1 and C$_{14}$Gua-HKUST-1 were stored in a desiccator (fig. S9) and characterised by PXRD, SEM and N$_2$ adsorption at intervals of 60, 90 and 150 days. Figure 3a-c show SEM images of C$_{12}$Gua-HKUST-1 after desiccator storage for these time periods providing valuable snapshots of the progress of the continual etching process. After 60 days (fig. 3a), the appearance of several randomly distributed isolated mesopores of diameter 10–40 nm are observed on the surface of the MOF crystals, which slightly increase in size and become significantly more numerous as storage time increases (fig. 3b,c). Similar results are observed for C$_{14}$Gua-HKUST-1 (fig S12); however, this is in stark contrast to pure HKUST-1 which displays apparently smooth crystal surfaces even after prolonged storage under the same conditions. (Fig. S13)
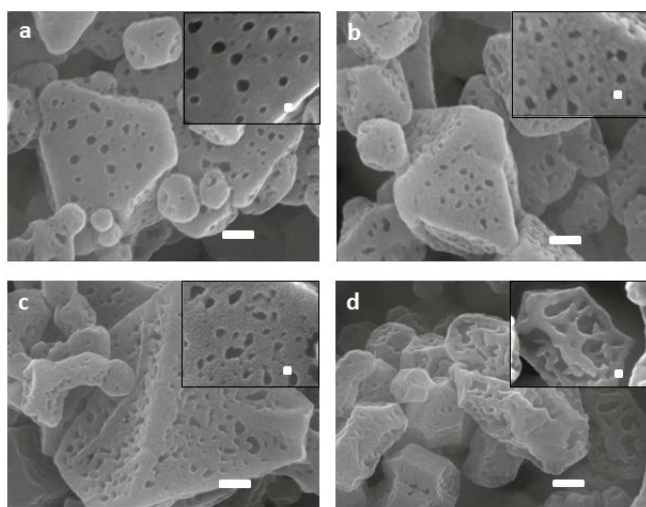

Figure 3. SEM images of C$_{12}$Gua-HKUST-1 stored in a desiccator for (a) 60, (b) 90 and (c) 150 days. The image shown in (d) is for the crystals removed from the desiccator after 60 days shown in (a), and stored in the laboratory atmosphere. Scale bars 100 nm and 10 nm (inset)

The C$_{12}$Gua-HKUST-1 desiccator samples were confirmed to be pure HKUST-1 by PXRD after all time periods (figure S14), and displayed the expected intermediate type I/IV isotherms (fig. S15, table S2) consistent with the appearance of mesopores on the surfaces of the crystals. The hysteresis loops for C$_{12}$Gua-HKUST-1(meso) observed on desorption were more pronounced than those for samples that had been left on the bench giving an average mesopore size of ~ 30 nm (as determined by the BJH model), in good agreement with the range determined by SEM (fig 3a-c). The BET surface area was found to be higher than the analogous bench-top sample, although much lower than C$_{12}$Gua-HKUST-1 with smooth surfaces obtained immediately following synthesis which displayed a type I isotherm (fig S16) due to its high degree of accessible microporosity. This further supports the TGA data

(fig S3 – S6) which indicate that the very small amounts of residual C$_n$Gua surfactants do not block the micropores.

Storage of the samples under low moisture conditions would thus appear to retard the formation of the meso- and macroscale surface patterns of C$_n$Gua-HKUST-1 (fig 3a-c) indicating that both the C$_n$Gua surfactants and water are required for the observed surface features to develop. This is further confirmed by allowing a sample of C$_{12}$Gua-HKUST-1(meso) prepared in a desiccator for 60 days to stand in the laboratory atmosphere. After a further 60 day period standing on the bench, there was a clear deterioration of the isolated mesopores which appeared to enlarge and join together producing meso-/macroscale features (fig 3d) like those previously observed. The appearance of these surface features was accompanied by a further reduction in BET surface area and micropore uptake (fig. S16, table S2) and a slight increase in mesopore size compared to C$_{12}$Gua-HKUST-1(meso). Similar observations were recorded for C$_{14}$Gua-HKUST-1(meso) (figs S16 - S18; table S3) and, as expected given the small difference in alkyl chain length between the C$_{12}$- and C$_{14}$Gua surfactants employed, the mesopore sizes are virtually identical for the various sample storage times.

Proposed mechanism of pattern formation

It is clear from the combined desiccator and bench-top studies of C$_n$Gua-HKUST-1 that the formation of the observed surface features is strongly dependent on both the C$_n$Gua surfactants used in the synthesis and subsequent access of water to the crystal surfaces. We postulate that the C$_n$Gua surfactants form nanoscale defects on the surfaces of the crystals that facilitate their post-synthetic etching by atmospheric water.

Prior to addition of the metal ion to the synthesis, the Gua headgroup forms strong interactions with some of the carboxylate groups of the BTC linkers. During framework formation the surfactants are largely restricted to the surface of the growing crystals due to phase separation resulting from relatively rapid formation of the stable HKUST-1 lattice.[9] This leads to the formation of nanoscale surface defects, where possible entanglement of C$_n$Gua alkyl chains precludes framework growth due to a space-filling effect. After almost complete removal of the surface-bound surfactants by washing, the exposed Cu(II) paddlewheel-terminated {111} faces of the octahedral crystals become highly susceptible to etching due to water coordination and linker displacement via ingress into the defects.[22] This initially forms isolated surface mesopores as the defects begin to hollow out (fig 3a), which eventually enlarge and amalgamate to form the observed meso- and macroscale patterns. As chain length increases the size of the (initial) surface defects is also likely to increase, which promotes a higher degree of etching and the formation of larger features during the same time period as clearly observed between the samples of C$_{10}$Gua-HKUST-1 and C$_{16}$Gua-HKUST-1. The etching process will inevitably lead to a partial collapse of the framework structure at the surface which will block access to the remaining bulk microporosity, resulting in the reduced BET surface areas and N$_2$ uptakes observed for the C$_n$Gua-HKUST-1 phases.

Nanoparticle growth of HKUST-1 by C$_{12}$Gua

In parallel to the above study, we also investigated the potential of further effects of C$_n$Gua surfactants on HKUST-1 formation by altering the order of addition, such that the metal ion was added to the surfactant solution prior to reaction with the ligand as shown in scheme 1 (path b). PXRD of the

products formed by stirring $Cu(OAc)_2$ with $C_{12}Gua$ in a 6:1 mole ratio followed by addition of BTC and solvothermal reaction show that HKUST-1 is formed. (Fig. S19) In this case the diffraction peaks are slightly broadened compared to $C_{12}Gua$-HKUST-1 (formed from ligand addition first), consistent with the formation of MOF nanoparticles. This is confirmed by SEM images which reveal that nanosized HKUST-1 crystallites of average size 60-80 nm are formed (fig 4, top), indicating that the particle size is readily tuneable from the micro- to the nanoscale simply by changing the order of addition. The manner in which the framework-forming components interact with the Gua surfactants are thus key to controlling the particle size, which clearly modulate the rates of nucleation and growth as previously observed for amphiphilic dodecanoic acid.[25] It is most likely that the cationic Gua headgroups form very strong interactions with the OAc^- anions from the Cu(II) precursor salt, effectively binding these to leave highly reactive Cu(II) species in solution where the increased chemical potential of the metal ion favours rapid nucleation and the formation of HKUST-1 nanoparticles upon addition of the BTC linker. Interactions between the OAc^- and the surfactant headgroup are further confirmed by the observation of a white precipitate on addition of the metal salt to the $C_{12}Gua$ solution and the absence of the amphiphile by TGA analysis. (Figure S20)
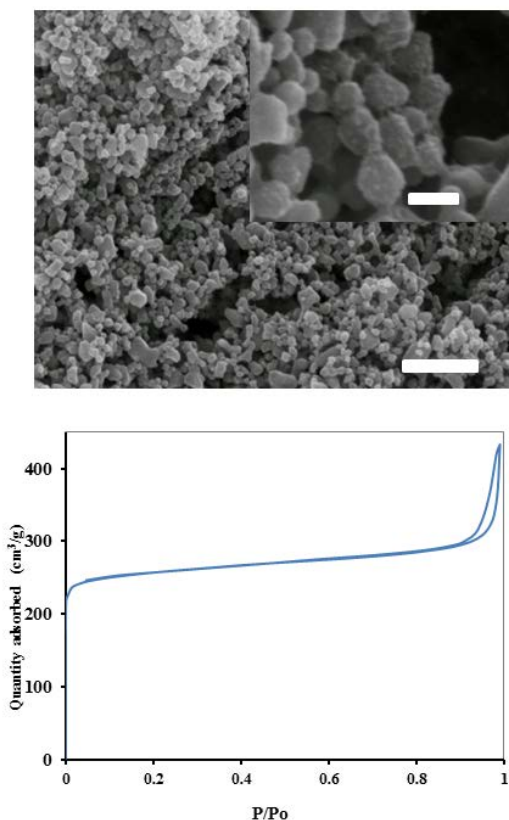

Figure 4. (Top) SEM images of HKUST-1 nanoparticles prepared via path b shown in scheme 1 (scale bars are 1 μm and 100 nm (inset)). (Bottom) N_2 adsorption-desorption isotherms at 77K of the HKUST-1 nanoparticles.

The N_2 adsorption-desorption isotherm of the nanosized HKUST-1 formed in the presence of $C_{12}Gua$ is shown in figure 4 (bottom). The data yield a BET surface area of 1018 m^2/g and a pore volume of 0.41 cm^3/g (at $p/p^0 = 0.3$) and 0.67 cm^3/g at

$p/p^0 = 0.99$ consistent with other reports of HKUST-1 nanoparticles and networks.[26] In addition, the isotherm reveals an increased N_2 uptake at high relative pressure and a modest desorption hysteresis centred at 50 nm (BJH). This is indicative of intergrain textural mesoporosity arising from the small particles observed in SEM images (fig 4, top).

Chromatography with surface-patterned $C_{14}Gua$-HKUST-1

In a previous study we demonstrated that the introduction of macropores into crystals of HKUST-1 via post-synthetic etching with hydroquinone could significantly improve the liquid phase separation of ethylbenzene and styrene when the hierarchically porous MOF is employed as a stationary phase in HPLC.[11a] Given the meso- and macroscale features on the surface of HKUST-1 prepared in the presence of C_nGua surfactants, we have also investigated the utility of C_nGua-HKUST-1 in HPLC. A column of $C_{14}Gua$-HKUST-1 was packed using our previously published procedure[11a] and conditioned with DCM for 24 hrs prior to use. Figure 5 shows the elution profiles for the separation of ethylbenzene and styrene for the $C_{14}Gua$-HKUST-1 column vs. a control column of pure smooth-surfaced HKUST-1 particles of comparable particle size. (Figure S21) The $C_{14}Gua$-HKUST-1 column has a consistent elution order and faster elution times for the two analytes (1.7 min for ethylbenzene and 2.9 min for styrene) compared to an analogous HKUST-1 control column and a recently reported HKUST-1@silica composite column[27], however the separation is not as pronounced for $C_{14}Gua$-HKUST-1. The increased adsorption kinetics for $C_{14}Gua$-HKUST-1 are due to the surface features arising from interactions with the $C_{14}Gua$ surfactants during synthesis, which results in a 25% reduction of column backpressure from 240 bars (smooth HKUST-1) to 187 bars.
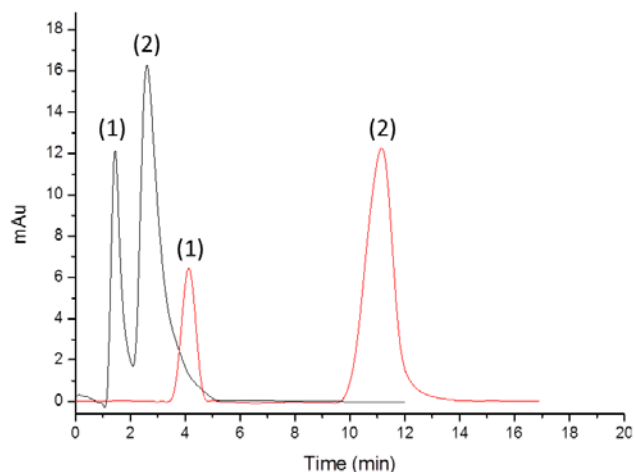

Figure 5. Comparison of the columns packed with pure HKUST-1 particles (red elution profile) and $C_{14}Gua$-HKUST-1 with meso-and macroscale surface features (black elution profile) for the HPLC separation of ethylbenzene (1) and styrene (2). Conditions: injection volume 1μL, flow rate 1 cm^3 min^{-1}, heptane:dichloromethane 98:2 v/v as the mobile phase.

As liquid-phase separation with highly microporous materials is largely a surface effect[28], the reduced separating power of the $C_{14}Gua$-HKUST-1 column is unsurprising. During pattern formation via etching of surface defects with atmospheric water the surface framework structure partially collapses: the resulting reduction in microporosity and the changing nature of the surface structure and/or composition will

thus have a big influence on the ability of the crystal surfaces to separate small molecules compared to the highly microporous and ordered surface presented by bulk (unmodified) HKUST-1. Despite this however, the separation of ethylbenzene and styrene with C_{14}Gua-HKUST-1 is better than commercial Basolite C300 (fig S22); however, this could be attributed to a difference in particle size between the two materials rather than the specific presence of surface features.

Conclusions

In order for small molecule additives to have an effect on MOF crystal growth kinetics, or for supramolecular assemblies to guide the formation of hierarchically porous MOF superstructures there needs to be a strong interaction with the framework building blocks. In this work we have demonstrated that by closely matching the supramolecular interactions between guanidinium-based amphiphiles and carboxylic acids novel meso- and macroscale surface features form on MOF crystals and nanoparticles are also accessible. This is strongly dependent on the order of addition of the reactants and thus allows us to control how the C_nGua surfactants interact with the MOF building blocks. In the former case, interaction between the C_nGua and the BTC linker of HKUST-1 during synthesis causes nanoscale surface defects to form which promote etching by adventitious water and the appearance of patterned surfaces. The post-synthetic etching by water of C_nGua-HKUST-1 is relatively slow; however, it is clear that this is promoted by supramolecular interactions and such a strategy could easily be combined with other etchant species *e.g.* hydroquinone or mild acid. By reversing the order of addition, the C_nGua species interact more strongly with the acetate group of the Cu(II) source, increasing the chemical potential of the metal to promote HKUST-1 nanoparticle formation. Surface patterning of the crystals appears to be a promising strategy to reduce the back pressure of columns when these crystals are employed as a stationary phase, although in the present case the dual templating-etching mechanism does degrade the surface. While this has an impact on overall column separation power, there is significant potential to tune this through optimal etchant selection.

Acknowledgements

Notes and references

[a] School of Chemistry, University of Southampton, Highfield Campus, Southampton SO17, 1BJ, U.K. E-mail: D.Bradshaw@soton.ac.uk. Tel. +44(0)2380599076.

[b] Dept of Chemistry, University of Liverpool, Crown St, Liverpool L69 7ZD, U.K.

† Electronic Supplementary Information (ESI) available: [details of any supplementary information available should be included here]. See DOI: 10.1039/b000000x/

1   (a) S. Kitagawa, R. Kitaura and S. Noro, *Angew. Chem., Int. Ed.*, 2004, **43**, 2334; (b) G. F´erey, *Chem. Soc. Rev.*, 2008, **37**, 191; (c) C. Janiak and J. K. Vieth, *New J. Chem.*, 2010, **34**, 2366; (d) D. Bradshaw, J. B. Claridge, E. J. Cussen, T. J. Prior and M. J. Rosseinsky, *Acc. Chem. Res.* 2005, **38**, 273.

2   (a) A. R. Millward and O. M. Yaghi, *J. Am. Chem. Soc.* 2005, **127**, 17998; (b) X. Lin, I. Telepeni, A. J. Blake, A. Dailly, C. M. Brown, J. M. Simmons, M. Zoppi, G. S. Walker, K. M. Thomas, T. J. Mays, P. Hubberstey, N. R. Champness and M. Schro¨der, *J. Am. Chem. Soc.*, 2009, **131**, 2159.

3   (a) J. Y. Lee, O. K. Farha, J. Roberts, K. A. Scheidt, S. T. Nguyen and J. T. Hupp, *Chem. Soc. Rev.* 2009, **38**, 1450; (b) A. Corma, H. Garcia and F. X. Llabre i Xamena, *Chem. Rev.*, 2010, **110**, 4606.

4   (a) S. Keskin and S. Kizilel, *Ind. Eng. Chem. Res.* 2011, **50**, 1799; (b) A. C. McKinlay, R. E. Morris, P. Horcajada, G. Fe´rey, R. Gref, P. Couvreur and C. Serre, *Angew. Chem., Int. Ed.*, 2010, **49**, 6260.

5   L. E. Kreno, K. Leong, O. K. Farha, M. D. Allendorf, R. P. Van Duyne and J. T. Hupp, *Chem. Rev.* 2012, **112**, 1105; (b) Z. Hu, B. J. Deibert and J. Li, *Chem. Soc. Rev.* 2014, DOI: 10.1039/c4cs00010b.

6   (a) Z. R. Herm, B. M. Wiers, J. A. Mason, J. M. van Baten, M. R. Hudson, P. Zajdel, C. M. Brown, N. Masciocchi, R. Krishna and J. R. Long, *Science* 2013, **340**, 960; (b) H. Bux, A. Feldhoff, J. Cravillon, M. Wiebcke, Y.-S. Li and J. Caro, *Chem. Mater.* 2011, **23**, 2262.

7   D. Bradshaw, A. Garai and J. Huo, *Chem. Soc. Rev.* 2012, **41**, 2344.

8   (a) Q.-R. Fang, T. A. Makal, M. D. Young and H.-C. Zhou, *Comments on Inorg Chem* 2010, **31**, 165; (b) W. Xuan, C. Zhu, Y. Liu and Y. Cui, *Chem. Soc. Rev.* 2012, **41**, 1677.

9   D. Bradshaw, S. El-Hankari and L. Lupica-Spagnolo, *Chem. Soc. Rev.* 2014, DOI: 10.1039/C4CS00127C.

10 L. Li, S. Xiang, S. Cao, J. Zhang, G. Ouyang, L. Chen and C.-Y. Su, *Nat. Commun.* 2013, **4**, 1774.

11 (a) A. Ahmed, N. Hodgson, M. Barrow, R. Clowes, C. M. Robertson, A. Steiner, P. McKeown, D. Bradshaw, P. Myers and H. Zhang, *J. Mater. Chem. A* 2014, DOI: 10.1039/C4TA00138A; (b) Y. Yue, Z.-A. Qiao, P. F. Fulvio, A. J. Binder, C. Tian, J. Chen, K. M. Nelson, X. Zhu, S. Dai, *J. Am. Chem. Soc.* 2013, **135**, 9572.

12 J. Reboul, S. Furukawa, N. Horike, M. Tsotsalas, K. Hirai, H. Uehara, M. Kondo, N. Louvain, O. Sakata and S. Kitagawa, *Nat. Mater.*, 2012, **11**, 717.

13 L.-G. Qiu, T. Xu, Z.-Q. Li, W. Wang, Y. Wu, X. Jiang, X.-Y Tian and L.-D. Zhang, *Angew. Chem., Int. Ed.*, 2008, **47**, 9487.

14 K. M. Choi, H. J. Jeon, J. K. Kang and O. M. Yaghi, *J. Am. Chem. Soc.* 2011, **133**, 11920.

15 S. S.-Y. Chui, S. M.-F. Lo, J. P. H. Charmant, A. G. Orpen and I. D. Williams, *Science*, 1999, **283**, 1148.

16 L. Alaerts, E. Seguin, H. Poelman, F. Thibault-Starzyk, P. A. Jacobs and D. E. De Vos, *Chem. Eur. J.* 2006, **12**, 7353.

17 Y. Liu, C. Hu, A. Comotti and M. D. Ward, *Science* 2011, **333**, 436.

18 J. A. Swift, A. M. Reynolds and M. D. Ward, *Chem. Mater.* 1998, **10**, 4159.

19 C. K. Lam, F. Xue, J.-P. Zhang, X.-M. Chen and T. C. W. Mak, *J. Am. Chem. Soc.* 2005, **127**, 11536.

20 V. N. Yadav and C. H. Gorbitz, *CrystEngComm* 2013, **15**, 439.

21 S. El-Hankari and P. Hesemann, *Eur. J. Inorg. Chem.* 2012, 5288.

22 (a) J. B. DeCoste, G. W. Peterson, B. J. Schindler, K. L. Killops, M. A. Browe and J. J. Mahle, *Journal of Materials Chemistry A*, 2013, **1**, 11922; (b) J. J. Low, A. I. Benin, P. Jakubczak, J. F. Abrahamanian, S. A. Faheem and R. R. Willis, *J. Am. Chem. Soc.* 2009, **131**, 15834.

23 (a) P. M. Schoenecker, C. G. Carson, H. Jasuja, C. J. J. Fleming and K. S. Walton, *Ind. Eng. Chem. Res.*, 2012, **51**, 6513; (b) P.

Kusgens, M. Rose, I. Senkovska, H. Frode, A. Henschel, S. Siegle and S. Kaskel, *Microporous Mesoporous Mater.*, 2009, **120**, 325.

24 Y. Yoo and H.-K. Jeong, *Chem. Eng. J.* 2012, **181-182**, 740.

25 S. Diring, S. Furukawa, Y. Takashima, T. Tsuruoka and S. Kitagawa, *Chem. Mater.*, 2010, **22**, 4531.

26 J. Huo, M. Brightwell, S. El-Hankari, A. Garai and D. Bradshaw, *J. Mater. Chem. A* 2013, **1**, 15220.

27 R. Ameloot, A. Liekens, L. Alaerts, M. Maes, A. Galarneau, B. Coq, G. Desmet, B. F. Sels, J. F. M. Denayer and D. E. de Vos, *Eur. J. Inorg. Chem.* 2010, 3735.

28 K. K. Unger, R. Skudas and M. M. Schulte, *J. Chromatogr. A* 2008, **1184**, 393.